Crystallization and Melting Behavior of Biodegradable Poly(ethylene succinate-*co*-6 mol % butylene succinate)

Yan Yang, Zhaobin Qiu

State Key Laboratory of Chemical Resource Engineering, Key Laboratory of Carbon Fiber and Functional Polymers, Ministry of Education, Beijing University of Chemical Technology, Beijing 100029, China

Received 21 October 2010; accepted 9 December 2010
DOI 10.1002/app.33881
Published online 19 April 2011 in Wiley Online Library (wileyonlinelibrary.com).

ABSTRACT: The crystallization, melting behavior, and spherulitic growth kinetics of biodegradable poly(ethylene succinate-*co*-6 mol % butylene succinate) [P(ES-*co*-6 mol % BS)] were investigated and compared with those of the homopolymer poly(ethylene succinate) (PES) in this work. The crystal structure of P(ES-*co*-6 mol % BS) was the same as that of neat PES, but the crystallinity decreased slightly because of the incorporation of the butylene succinate content. The glass-transition temperature decreased slightly for P(ES-*co*-6 mol % BS) compared to that for neat PES. The melting point of P(ES-*co*-6 mol % BS) decreased apparently; moreover, the equilibrium melting point was also reduced. Two melting endotherms were found for P(ES-*co*-6 mol % BS) after isothermal crystallization; this was ascribed to the melting, recrystallization, and remelting mechanism. The spherulitic growth rate of P(ES-*co*-6 mol % BS) was slower than that of neat PES at a given crystallization temperature. Both neat PES and P(ES-*co*-6 mol % BS) exhibited a crystallization regime II to III transition; moreover, the crystallization regime transition temperature of P(ES-*co*-6 mol % BS) shifted to a low temperature compared with that of neat PES. © 2011 Wiley Periodicals, Inc. J Appl Polym Sci 122: 105–111, 2011

Key words: crystallization; morphology; thermal properties

INTRODUCTION

Biodegradable polymers have attracted more and more attention from the viewpoints of environmental protection and resource recycling. Two main kinds of biodegradable polymers have been investigated, namely, biosynthetic biodegradable polymers and chemosynthetic biodegradable polymers. On the one hand, bacterial polyhydroxyalkanoates are typical biosynthetic biodegradable polymers, and some examples include poly(3-hydroxybutyrate) and poly(3-hydroxybutyrate-*co*-3-hydroxylvalerate). On the other hand, aliphatic polyesters are usually chemosynthetic biodegradable polymers, and some examples include poly(L-lactide) and poly (ε-caprolactone).

Correspondence to: Z. Qiu (qiuzb@mail.buct.edu.cn).

Contract grant sponsor: National Natural Science Foundation, China; contract grant numbers: 20774013, 20974012.

Contract grant sponsor: Fundamental Research Funds for the Central Universities; contract grant number: ZZ1005.

Contract grant sponsor: Program for Changjiang Scholars and Innovative Research Team in University; contract grant number: IRT0706.

Poly(ethylene succinate) (PES) is a linear aliphatic biodegradable polyester with a chemical structure of $-(OCH_2CH_2O_2CCH_2CH_2CO)-_n$. It is one of the most promising chemosynthetic biodegradable polymers and has already drawn considerable attention in recent decades. The crystallization behavior, spherulitic morphology and growth kinetics, melting behavior, and degradation of PES have been investigated extensively.[1–12] Many investigations on modification through physical polymer blending and chemical copolymerization have also been reported to extend the practical application fields of PES. Usually, polymer blending is a convenient and economical method for designing new materials with desired properties. PES has been already blended with many polymers, including poly (ethylene oxide), poly(L-lactide), poly(ε-caprolactone), poly(vinyl phenol), and poly(3-hydroxybutyrate).[13–19] Meanwhile, various properties of PES have also been modified via chemical copolymerization, namely, the incorporation of a second comonomer into the backbone of neat PES. Superior mechanical properties can be achieved easily because a much better miscibility for the two compositions is provided.[20–25]

Similar to PES, poly(butylene succinate) is also biodegradable polyester;[7] thus, through the incorporation of the second comonomer butylene succinate (BS) into the backbone of PES, some novel completely biodegradable copolymers, poly(ethylene succinate-*co*-

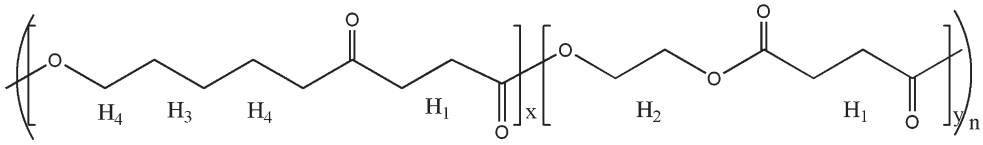

Scheme 1 Chemical structure of P(ES-*co*-6 mol % BS).

butylene succinate)s, may be developed. It is clear that the amount of BS should be small if a relatively high melting temperature (T_m) is required for the copolyesters. Therefore, the crystal structure, melting behavior, and spherulitic morphology and growth kinetics of biodegradable poly(ethylene succinate-*co*-6 mol % butylene succinate) [P(ES-*co*-6 mol % BS)] were investigated in detail and compared with those of neat PES in this work. It is expected that the results reported herein will be of interest and help provide a better understanding of the relationship between the structure and properties of biodegradable polymers.

EXPERIMENTAL

PES (weight-average molecular weight = 4.65×10^4) and P(ES-*co*-6 mol % BS) (weight-average molecular weight = 5.33×10^4) used in this study were synthesized by a two-step melt-polycondensation method.[20,21] The chemical structure of P(ES-*co*-6 mol % BS) is shown in Scheme 1.

Wide-angle X-ray diffraction (WAXD) experiments were performed on a Rigaku d/Max2500 VB2+/PC X-ray diffractometer (Tokyo, Japan) at 40 kV and 20 mA at 4°/min. The samples for the WAXD experiments were first pressed into films with thicknesses of around 1 mm on a hot stage at 140°C for 2 min and then transferred into an oven at 60°C for 24 h.

Thermal analysis was performed with a TA Instruments differential scanning calorimeter (Q100) (New Castle, Delaware, USA) with Universal Analysis 2000. The glass-transition temperature (T_g) and T_m of the melt-quenched samples were measured at a heating rate of 20°C/min. The samples were first annealed at 140°C for 3 min to erase any thermal history and were subsequently quenched to −70°C at a cooling rate of 60°C/min. The isothermal melt crystallization was also examined with differential scanning calorimetry (DSC). The samples were first heated to 140°C for 3 min and then cooled at 60°C/min to the desired crystallization temperature (T_c) until the crystallization was complete. After isothermal melt crystallization, the samples were heated to the melt again at 20°C/min to study the subsequent melting behavior. All operations were performed under nitrogen purge, and the sample weight varied between 4 and 5 mg.

The spherulitic morphology and growth kinetics of neat PES and P(ES-*co*-6 mol % BS) were investigated with a polarized optical microscope (Olympus BX51) (Tokyo, Japan) equipped with a temperature controller (Linkam THMS 600). The samples were first melted at 140°C for 3 min to erase any thermal history and then quenched to the desired T_c's at 60°C/min. The spherulitic growth rate (G) was calculated from the variation of the radius (R) with time (t), that is, $G = dR/dt$.

RESULTS AND DISCUSSION

Crystal structure of P(ES-*co*-6 mol % BS)

It was interesting to study the influence of the BS composition on the crystal structure of PES. The crystal structure of P(ES-*co*-6 mol % BS) was investigated with WAXD and compared with that of neat PES. Figure 1 shows the WAXD patterns of P(ES-*co*-6 mol % BS) and neat PES isothermally crystallized at 60°C for 24 h. The crystal structure of PES was orthorhombic,[26,27] and the diffraction peaks observed at 20.2 and 23.4° were from (120) and (200) planes, respectively. It was apparent that the diffraction peak at 20.2° moved a little toward a higher degree, whereas the peak at 23.4° was almost at the same location; this suggested that the introduction of the BS content did not change the crystal structure of PES in the copolyester. It can be explained that the BS content may have existed in an amorphous state and was excluded from the crystal region of PES.[28]

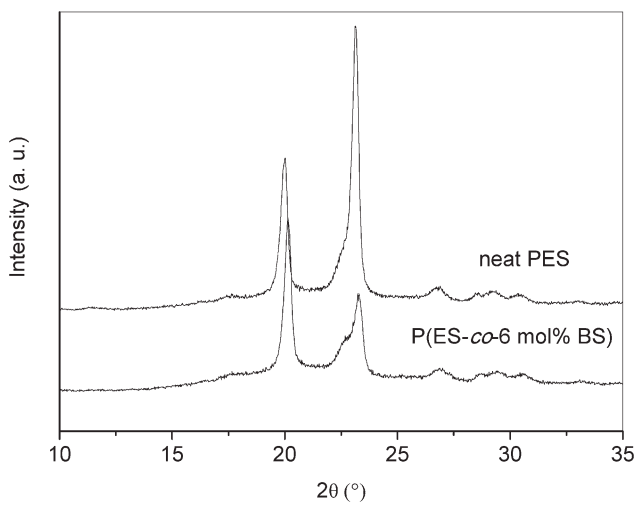

Figure 1 WAXD patterns of neat PES and P(ES-*co*-6 mol % BS).

TABLE I
Summary of the Basic Thermal Properties for Neat PES and P(ES-*co*-6 mol % BS)

Sample	T_g (°C)	T_{ch} (°C)	ΔH_{ch} (J/g)	T_m (°C)	ΔH_m (J/g)	X_c (%)
Neat PES	−11.3	31.2	50.8	102.5	65.9	58.4
P(ES-*co*-6 mol % BS)	−12.7	31.3	45.9	95.9	55.0	42.3

Even though the locations of the two main diffraction peaks were almost unchanged, the intensities of the diffraction peaks decreased obviously because of the BS content; this indicated that the incorporation of the BS content reduced the crystallinity (X_c) compared to that of neat PES. From Figure 1, the values of X_c of neat PES and P(ES-*co*-6 mol % BS) were 58.4 and 42.3%, respectively, and they are listed in Table I for comparison.

Basic thermal properties of P(ES-*co*-6 mol % BS)

As introduced in the Experimental section, T_g and T_m were detected at a heating rate of 20°C/min for the melt-quenched P(ES-*co*-6 mol % BS) and compared with those of neat PES. Figure 2 shows the DSC heating traces of neat PES and P(ES-*co*-6 mol % BS). Neat PES had a T_g of around −11.3°C and a T_m of 102.5°C with a melting enthalpy (ΔH_m) of 65.9 J/g, whereas P(ES-*co*-6 mol % BS) had a T_g around −12.7°C and a T_m of 95.9°C with a ΔH_m around 55.0 J/g. It was clear that T_g of P(ES-*co*-6 mol % BS) was very close to that of neat PES; this indicated that a small amount of BS exerted little influence on the mobility of PES. However, it could also be seen that T_m of P(ES-*co*-6 mol % BS) was depressed when compared with that of neat PES; this suggested that the crystallization behavior of P(ES-*co*-6 mol % BS) was hindered because of the copolymerization with the BS composition. It should be noted that a cold crystallization peak temperature (T_{ch}) of around 31.3°C with a cold crystallization enthalpy (ΔH_{ch}) of 45.9 J/g was detected for P(ES-*co*-6 mol % BS). Moreover, it could be seen that T_{ch} with a ΔH_{ch} around 50.8 J/g for neat PES was much sharper than that of P(ES-*co*-6 mol % BS), regardless of the almost unchanged T_{ch}. It should also be noted that there existed an exothermal peak at about 80°C before the melting peak for both neat PES and P(ES-*co*-6 mol %BS); this may have been due to the melting and recrystallization of the unstable crystals formed during the cold crystallization.[1] All of the obtained T_g, T_{ch}, ΔH_{ch}, T_m, and ΔH_m values are summarized in Table I for comparison.

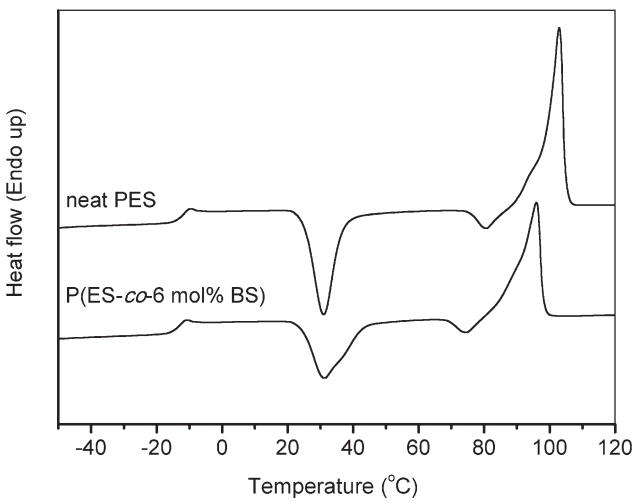

Figure 2 DSC heating curves of neat PES and P(ES-*co*-6 mol % BS) at 20°C/min after quenching from the melt at 60°C/min.

Multiple melting behaviors and equilibrium melting temperature (T_m^o) of P(ES-*co*-6 mol % BS)

As described in the Experimental section, the melting behavior of P(ES-*co*-6 mol % BS) was studied with DSC. As displayed in Figure 3, two melting endothermic peaks, denoted as T_{m1} and T_{m2} from low to high temperatures, were observed in a range of T_c's for P(ES-*co*-6 mol % BS). T_{m1} shifted from around 79.3 to 86.6°C with increasing T_c from 55 to 65°C; however, T_{m2} was almost unchanged around 95°C. Furthermore, the ratio of the area of T_{m1} to that of T_{m2} increased with increasing T_c. For example, the values of the two melting enthalpies corresponding to T_{m1} and T_{m2} were around 4.5 and 43.5 J/g, respectively, at T_c = 55°C; thus, the ratio of the

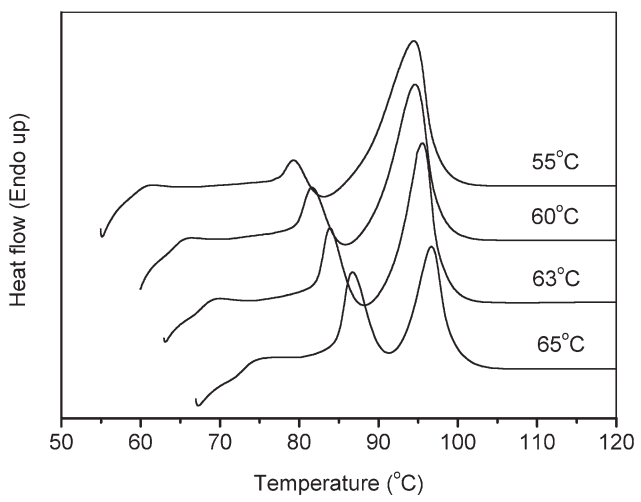

Figure 3 Melting behaviors of P(ES-*co*-6 mol % BS) crystallized at various T_c's.

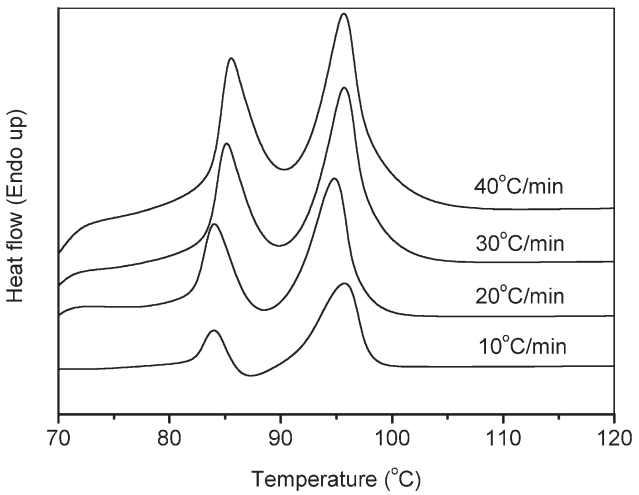

Figure 4 Melting behaviors of P(ES-*co*-6 mol % BS) crystallized at 65°C at different heating rates.

area of T_{m1} to that of T_{m2} was around 0.103. At T_c = 60°C, the values of the two melting enthalpies corresponding to T_{m1} and T_{m2} were around 9.4 and 40.4 J/g, respectively; thus, the ratio of the area of T_{m1} to that of T_{m2} increased to be around 0.232. These facts may be explained by the mechanism of melting, recrystallization, and remelting of P(ES-*co*-6 mol % BS) crystals.[29–31] T_{m1} was the melting of the crystals formed at T_c that were present before the heating scan in DSC, and T_{m2} was the melting of the crystals formed through the recrystallization and reorganization of the crystals corresponding to T_{m1}.

The scanning rate dependence on the multiple melting behaviors is often considered as solid evidence to explain the melting, recrystallization, and remelting model. Figure 4 displays the scanning rate dependence of the melting behavior of P(ES-*co*-6 mol % BS) crystallized completely at 65°C. From Figure 4, two melting endothermic peaks, denoted as T_{m1} and T_{m2} from low to high temperatures, were observed in a range of heating rates for P(ES-*co*-6 mol % BS). With the increase of the heating rate, T_{m1} shifted to a high-temperature range, whereas T_{m2} was almost unchanged; furthermore, the values of $\Delta H_{m2}/\Delta H_{m1}$ decreased with increasing scanning rate from 10 to 40°C/min. The results relate to the fact that less time was available for the recrystallization as a result of the increased heating rate. Briefly, with increasing scanning rate, the recrystallization of P(ES-*co*-6 mol % BS) was inhibited. Similar results were also found for poly(butylene succinate).[7]

It is well known that both the thermodynamic factors and the morphological factors, such as crystalline lamellar thickness, affect T_m of a semicrystalline polymer. For a better understanding of the effect of the BS content on the T_m depression of P(ES-*co*-6 mol % BS), the T_m^o should be obtained to separate the morphological effects from the thermodynamic effects.

Hoffman and Weeks proposed a relationship between the apparent T_m and the isothermal T_c as follows:

$$T_m = \eta T_c + (1 - \eta) T_m^o \quad (1)$$

where T_m^o is the equilibrium melting point and η is a measurement of the stability, that is, the lamellar thickness, of the crystals undergoing the melting process.[32] T_m^o can thus be obtained from the intersection of this line with the $T_m = T_c$ equation.

For the reasons listed previously, T_{m1} was used for the analysis of the Hoffman–Weeks equation. Figure 5 displays the Hoffman–Weeks plots for neat PES and P(ES-*co*-6 mol % BS). From Figure 5, T_m^o was determined to be around 117.8°C for neat PES. In the case of its copolyester P(ES-*co*-6 mol % BS), the value of T_m^o was around 104.8°C. Clearly, the incorporation of BS led to a significant depression of T_m^o of P(ES-*co*-6 mol % BS).

Spherulitic morphology and growth kinetics of P(ES-*co*-6 mol % BS)

The spherulitic morphology and growth kinetics of P(ES-*co*-6 mol % BS) were investigated further because they may have influenced the final physical properties and biodegradation of P(ES-*co*-6 mol % BS). Figure 6 presents the polarized optical microscopy (POM) images of neat PES and P(ES-*co*-6 mol % BS) isothermally crystallized at 60°C as an example. From these images, it was apparent that the sizes of the spherulites of P(ES-*co*-6 mol % BS) were larger than those of neat PES; this suggested that the nucleation density of the spherulites decreased in P(ES-*co*-6 mol % BS) compared to that of neat PES. Such results indicate that the copolymerization with BS made the nucleation more difficult for P(ES-*co*-6 mol % BS) than for neat PES at a given T_c. However, it should be noted that the supercooling was

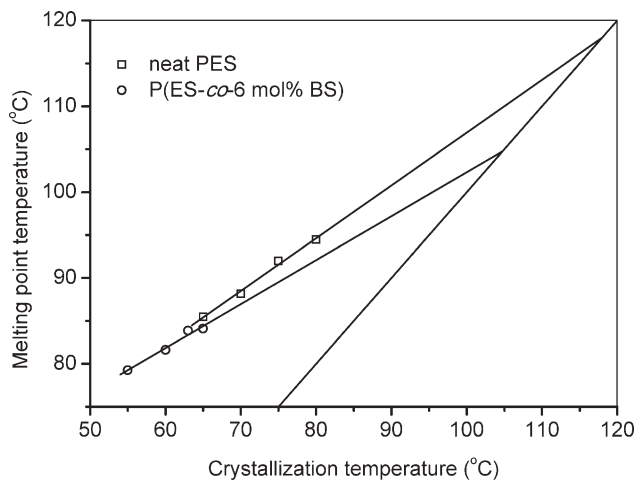

Figure 5 Hoffman–Weeks plots for the determination of T_m^o's of neat PES and P(ES-*co*-6 mol % BS).

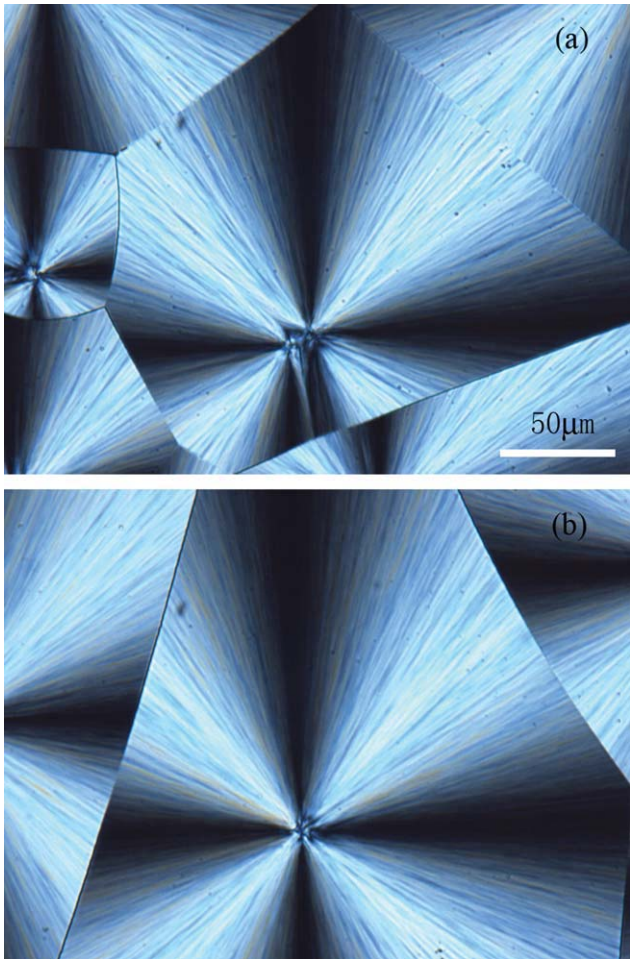

Figure 6 Spherulitic morphology of neat PES and P(ES-*co*-6 mol % BS) crystallized at 60°C (same scale bar = 50 μm): (a) neat PES and (b) P(ES-*co*-6 mol % BS). [Color figure can be viewed in the online issue, which is available at wileyonlinelibrary.com.]

different for the two samples, despite the same T_c because of the difference in T_m^o. Therefore, the aforementioned results were related to the fact that the degree of supercooling (ΔT) of P(ES-*co*-6 mol % BS) was smaller than that of neat PES as a result of the depression of T_m^o of P(ES-*co*-6 mol % BS).

We calculated the growth rates of the spherulites by following the development of radius with time at various T_c's in this work with POM. Both neat PES and P(ES-*co*-6 mol % BS) spherulites showed a linear growth with crystallization time until contact with other spherulites during crystallization. Figure 7 shows the temperature dependence of G for neat PES and P(ES-*co*-6 mol % BS). From Figure 7, it is obvious that the curves of both neat PES and P(ES-*co*-6 mol % BS) showed a good bell shape. The G values of both neat PES and P(ES-*co*-6 mol % BS) first increased with increasing T_c and then started to decrease with further increasing T_c after they reached the maximum; moreover, G of neat PES was rather faster than that of P(ES-*co*-6 mol % BS) at a given T_c. The reduction in the G of P(ES-*co*-6 mol % BS) may have been related to the following factors, that is, the lower thermodynamic driving force required for the growth of spherulites and the diluent effect of the BS content in the copolymer.

To further study the spherulitic growth kinetics of P(ES-*co*-6 mol % BS), the secondary nucleation theory, which is usually called the *Lauritzen–Hoffman equation*, was applied in this work to analyze the G values of neat PES and P(ES-*co*-6 mol % BS). On the basis of this theory,[33] G at a given T_c is expressed by the following equation:

$$G = Go \exp\left[-\frac{U*}{R(Tc - T\infty)}\right] \exp\left[-\frac{Kg}{Tc(\Delta T)f}\right] \quad (2)$$

where G_o is a preexponential factor, U^* is the activation energy for transporting the polymer chain segments to the crystallization site, R is the gas constant, T_∞ is a temperature below which the polymer chain movement ceases, ΔT is the degree of supercooling described as $T_m^o - T_c$, f is a correction factor accounting for the variation in the enthalpy of fusion given as $f = 2T_c/(T_m^o + T_c)$, and K_g is the nucleation constant, given as follows:

$$K_g = \frac{mbo\sigma\sigma eTm^\circ}{\Delta hfk} \quad (3)$$

where σ and σ_e are the lateral surface free energy and end-surface free energy, respectively; b_o is the molecular thickness; Δh_f is the heat of fusion per unit volume; and k is the Boltzmann constant, and the value of m is a constant, which is equal to 2 or 4 depending on crystallization regime. For practical convenient use, eq. (2) is usually rewritten as follows:

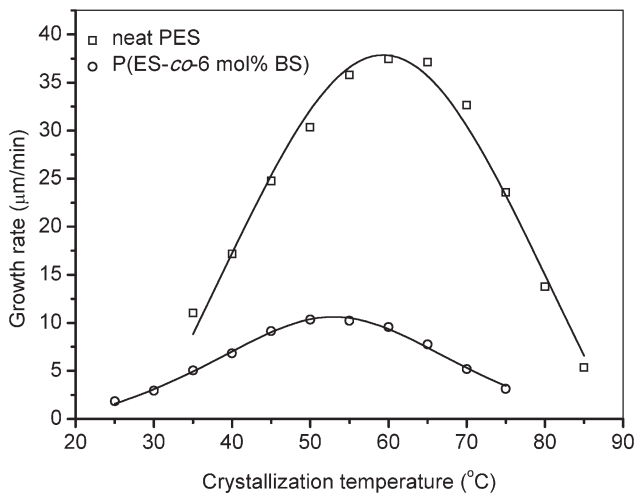

Figure 7 Variation of G with T_c for neat PES and P(ES-*co*-6 mol % BS).

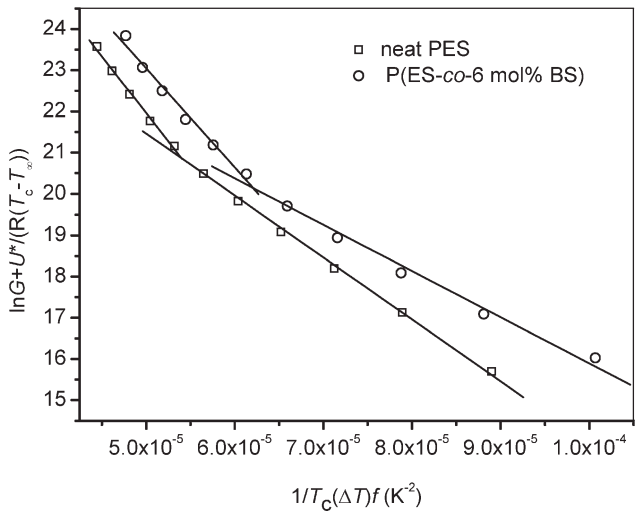

Figure 8 Lauritzen–Hoffman plots of neat PES and P(ES-*co*-6 mol % BS).

$$\ln G + \frac{U*}{R(Tc - T\infty)} = Go - \frac{Kg}{Tc(\Delta T)f} \quad (4)$$

To understand how the nucleation process affects the crystalline morphology, two important processes and their rates should be considered. Hoffman predicted the following three crystallization regimes.[33] In crystallization regime I, the rate of spreading is much greater than the rate of secondary nucleation; therefore, once a nucleus has formed, it will spread rapidly across a substrate length on the growth front. In crystallization regime II, the rate of spreading is comparable to the rate of secondary nucleation; therefore, several nuclei may form and spread across the substrate together. In crystallization regime III, the rate of secondary nucleation is much greater than the rate of spreading; therefore, the separation of nuclei is comparable with the molecular width so that no spreading occurs. The theoretical m values were 4, 2, and 4 for $K_g^{I/II}$, $K_g^{II/III}$, and $K_g^{I/III}$, respectively. Values of $U^* = 17246.3$ J/mol and $T_\infty = T_g - 51.6$ K were used in this work.[34] Figure 8 displays the Lauritzen–Hoffman plots for neat PES and P(ES-*co*-6 mol % BS), respectively. It can be seen from Figure 8 that the parameters of U^* and T_∞ could be well fitted with two straight lines with different slopes in a wide range of T_c's. On the basis of the Lauritzen–Hoffman theory, such discontinuity should have been attributed to a transition from regime II at high T_c to regime III at low T_c. K_g^{II} and K_g^{III} were obtained from the two slopes of each line for neat PES and P(ES-*co*-6 mol % BS). The values of K_g^{III}/K_g^{II} were about 1.8 and 2.1 for neat PES and P(ES-*co*-6 mol % BS), respectively. From the results mentioned previously, the regime transition temperatures (T_{tr}) for neat PES and P(ES-*co*-6 mol % BS) were around 57 and 52°C, respectively. T_{tr} decreased with the introduction of the BS composition. As shown in the previous section, the difference in T_g between neat PES and P(ES-*co*-6 mol % BS) was only about 1.5°C, whereas the difference in T_m^o between the two components was 13°C. Therefore, the shift of T_{tr} toward lower temperature with the incorporation of the BS composition was probably related to the depression of T_m^o of P(ES-*co*-6 mol % BS). Similar results have also been reported for other polymers.[35,36]

CONCLUSIONS

The crystal structure, melting behavior, spherulitic morphology, and growth kinetics of the biodegradable copolymer P(ES-*co*-6 mol % BS) were investigated with WAXD, DSC, and POM in detail and were compared with those of neat PES in this work. The WAXD results indicate that the incorporation of BS content did not modify the crystal structure but decreased X_c of P(ES-*co*-6 mol % BS) as compared to that of neat PES. The basic thermal properties and multiple melting behaviors were studied with DSC. In the presence of the BS composition, T_g decreased slightly and T_m decreased apparently for P(ES-*co*-6 mol % BS). Double melting behavior was found for P(ES-*co*-6 mol % BS) after isothermal crystallization, which may have been due to the melting, recrystallization, and remelting mechanism. T_m^o of P(ES-*co*-6 mol % BS) was reduced obviously because of the incorporation of the BS composition. The spherulitic morphologies of neat PES and P(ES-*co*-6 mol % BS) were observed with POM in a wide range of T_c's. The G values of neat PES and its copolyester were also measured as a function of T_c. Bell-shaped curves were found for the growth rate for both neat PES and P(ES-*co*-6 mol % BS). At a given T_c, G was slower in P(ES-*co*-6 mol % BS) than in neat PES. On the basis of Lauritzen and Hoffman theory, the G values of P(ES-*co*-6 mol % BS) were further analyzed and compared with that of neat PES. Both neat PES and P(ES-*co*-6 mol % BS) exhibited a crystallization regime II to III transition; furthermore, T_{tr} shifted to a low-temperature range with the introduction of the BS composition.

References

1. Qiu, Z.; Ikehara, T.; Nishi, T. Polymer 2003, 44, 5429.
2. Gan, Z.; Abe, H.; Doi, Y. Biomacromolecules 2000, 1, 713.
3. Papageorgiou, G.; Bikiaris, D.; Achilias, D. Thermochim Acta 2007, 457, 41.
4. Qiu, Z.; Fujinami, S.; Komura, M.; Nakajima, K.; Ikehara, T.; Nishi, T. Polym J 2004, 36, 642.
5. Ichikawa, Y.; Noguchi, K.; Okuyama, K.; Washiyama, J. Polymer 2001, 42, 3703.
6. Gan, Z.; Abe, H.; Doi, Y. Biomacromolecules 2000, 1, 704.

7. Qiu, Z.; Komur, M.; Ikehara, T.; Nishi, T. Polymer 2003, 44, 7781.
8. Caminiti, R.; Isopo, A.; Orru, M.; Albertini, V. Chem Mater 2000, 12, 369.
9. Gan, Z.; Abe, H.; Doi, Y. RIKEN Rev 2001, 42, 11.
10. Tezuka, Y.; Ishii, N.; Kasuya, K.; Mitomo, H. Polym Degrad Stab 2004, 84, 115.
11. Iwata, T.; Doi, Y. Macromolecules 2001, 34, 7343.
12. Chrissafis, K.; Paraskevopoulos, K.; Bikiaris, D. Thermochim Acta 2005, 435, 142.
13. Chen, H.; Wang, S. Polymer 2000, 41, 5157.
14. Lu, J.; Qiu, Z.; Yang, W. Polymer 2007, 48, 4196.
15. Qiu, Z.; Ikehara, T.; Nishi, T. Macromolecules 2002, 35, 8251.
16. Lu, J.; Qiu, Z.; Yang, W. Macromolecules 2008, 41, 141.
17. Seretoudi, G.; Bikiaris, D.; Panayiotou, C. Polymer 2002, 43, 5405.
18. Al-Salah, H. Polym Bull 1998, 41, 593.
19. Qiu, Z.; Fujinami, S.; Komura, M.; Nakajima, K.; Ikehara, T.; Nishi, T. Polymer 2004, 45, 4515.
20. Lu, H.; Lu, S.; Chen, M.; Chen, C.; Tsai, C. J Appl Polym Sci 2009, 113, 876.
21. Chen, C.; Lu, H.; Chen, M.; Peng, J.; Tsai, C.; Yang, C. J Appl Polym Sci 2009, 111, 1433.
22. Cao, A.; Okamura, T.; Nakayama, K.; Inoue, Y.; Masuda, T. Polym Degrad Stab 2002, 78, 107.
23. Mochizuki, M.; Mukai, K.; Yamada, K.; Ichise, N. Ichise, N. Murase, S.; Iwaya, Y. Macromolecules 1997, 30, 7403.
24. Chen, M.; Chang, W.; Lu, H.; Chen, C.; Peng, J.; Tsai, C. Polymer 2007, 48, 5408.
25. Papageorgiou, G.; Bikiaris, D. Macromol Chem Phys 2009, 210, 1408.
26. Gan, Z.; Abe, H.; Kurokawa, H.; Doi, Y. Biomacromolecules 2001, 2, 605.
27. Ueda, A.; Chatani, Y.; Tadokoro, H. Polym J 1971, 2, 387.
28. Ichikawa, Y.; Washiyama, J.; Moteki, Y.; Noguchi, K.; Okuyama, K. Polym J 1995, 27, 1264.
29. Qiu, Z.; Ikehara, T.; Nishi, T. Polymer 2003, 44, 3095.
30. Qiu, Z.; Komura, M.; Ikehara, T.; Nishi, T. Polymer 2003, 44, 8111.
31. Liu, T.; Petermann, J. Polymer 2001, 42, 6453.
32. Hoffman, J.; Weeks, J. J Chem Phys 1965, 42, 4301.
33. Hoffman, J.; Davis, G.; Lauritzen, J. In Treatise on Solid State Chemistry; Hannay, N. B., Ed.; Plenum: New York, 1976; Vol. 3, Chapter 7.
34. Williams, M.; Landel, R.; Ferry, J. J Am Chem Soc 1955, 77, 3701.
35. Gan, Z.; Abe, H.; Doi, Y. Biomacromolecules 2001, 2, 313.
36. Cai, H.; Qiu, Z. Phys Chem Chem Phys 2009, 11, 9569.